

**This is the accepted manuscript version of the contribution published as:**

**Ji, L., Ji, S., Wang, C., Kepp, K.P. (2018):**

Molecular mechanism of alternative P450-catalyzed metabolism of environmental phenolic endocrine-disrupting chemicals

*Environ. Sci. Technol.* **52** (7), 4422 – 4431

**The publisher's version is available at:**

<http://dx.doi.org/10.1021/acs.est.8b00601>



## 17 **Abstract**

18 Understanding the bioactivation mechanisms to predict toxic metabolites is critical for risk  
19 assessment of phenolic endocrine-disrupting chemicals (EDCs). One mechanism involves *ipso*-  
20 substitution, which may contribute to the total turnover of phenolic EDCs, yet the detailed  
21 mechanism and its relationship with other mechanisms are unknown. We used density functional  
22 theory to investigate the P450-catalyzed *ipso*-substitution mechanism of the prominent  
23 xenoestrogen bisphenol A. The *ipso*-substitution proceeds via H-abstraction from bisphenol A by  
24 Compound I, followed by essentially barrierless OH-rebound onto the *ipso*-position forming a  
25 quinol, which can spontaneously decompose into the carbocation and hydroquinone. This  
26 carbocation can further evolve into the highly estrogenic hydroxylated and dimer-type metabolites.  
27 The H-abstraction/OH-rebound reaction mechanism has been verified as a general reaction mode  
28 for many other phenolic EDCs, such as bisphenol analogues, alkylphenols and chlorophenols. The  
29 identified mechanism enables us to effectively distinguish between type I (eliminating-substituent  
30 as anion) and type II (eliminating-substituent as cation) *ipso*-substitution in various phenolic  
31 EDCs. We envision that the identified pathways will be applicable for prediction of metabolites  
32 from phenolic EDCs whose fate is affected by this alternative type of P450 reactivity, and  
33 accordingly enable the screening of these metabolites for endocrine-disrupting activity.

34

35

36

37

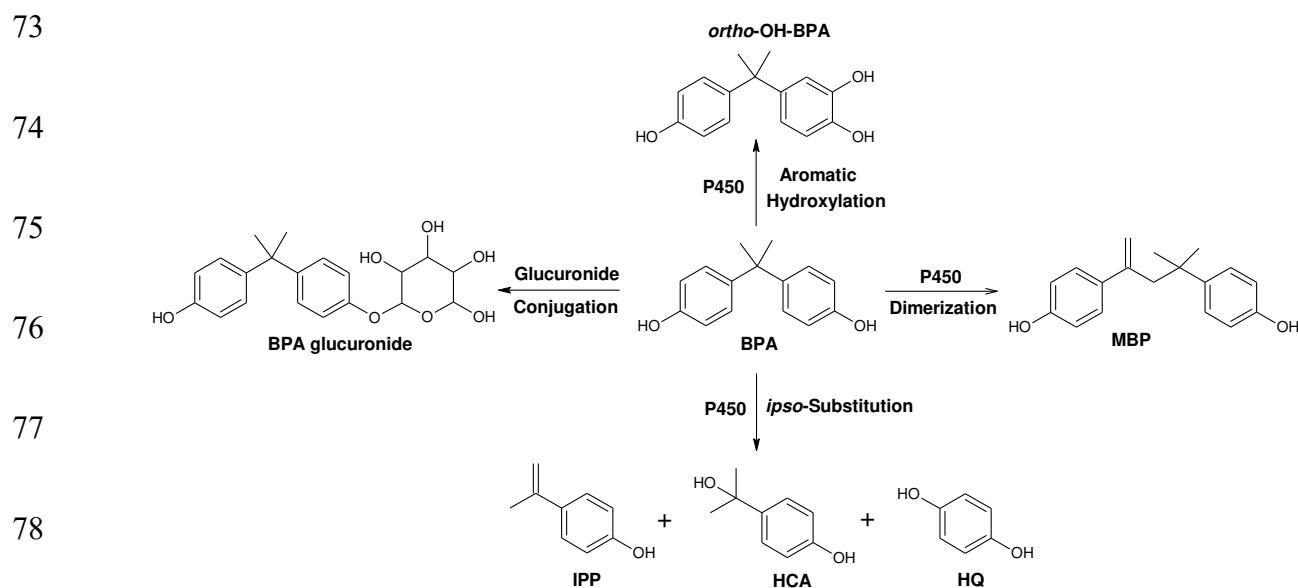
## 38 **Introduction**

39 Biotransformation plays a critical role in determining the toxicity of xenobiotics in organisms and  
40 has drawn considerable attention as a basis for environmental risk assessment.<sup>1,2</sup>  
41 Biotransformation of environmental endocrine-disrupting chemicals (EDCs) is one such  
42 example.<sup>3,4</sup> Accurate risk assessment of EDCs requires consideration of bioactivation via  
43 biotransformation processes, especially by human cytochrome P450 enzymes (P450), since  
44 neglecting these metabolic pathways may lead to undervaluation of their adverse effects on human  
45 health, although the metabolism of phenolic chemicals by P450 is minor compared with the  
46 glucuronidation pathway under normal circumstances.<sup>3,4</sup> P450 enzymes are a superfamily of  
47 monooxygenases distributed through all kingdoms of life, and are responsible for most phase-I  
48 biotransformation reactions.<sup>5-9</sup> Some of these conversions produce metabolites that are much more  
49 toxic than their parent compounds, an important example being phenolic EDCs.<sup>10</sup> Phenolic EDCs  
50 such as bisphenol analogues, alkylphenols and chlorophenols, are ubiquitous in the environment  
51 as widely used industrial chemicals, with associated high risk of environmental exposure.<sup>10</sup> Among  
52 these, although bisphenol A (BPA) has traditionally been considered a weak environmental  
53 xenoestrogen because of its much lower binding affinity to the estrogen receptor than that of  
54 estradiol,<sup>11</sup> the biotransformation largely affects the endocrine disrupting activity of BPA.<sup>4</sup>

55 As shown in **Scheme 1**, conjugation with the phase II glucuronide enzyme is the predominant  
56 metabolic pathway of BPA in humans (more than 90% of all BPA metabolites), which represents  
57 a major detoxification pathway;<sup>12</sup> however, BPA is also metabolized by human P450 to form  
58 *ortho*-OH-BPA via hydroxylation of the aromatic ring,<sup>12</sup> to form hydroxycumyl alcohol (HCA),  
59 isopropenylphenol (IPP), and hydroquinone (HQ) via an *ipso*-substitution mechanism,<sup>13</sup> and to  
60 form a dimer-type metabolite 4-methyl-2,4-bis(4-hydroxyphenyl)pent-1-ene (MBP) whose

61 formation may involve IPP reacting with isopropenylphenol radical.<sup>14,15</sup> *In vitro* assays have  
62 shown that HCA can exhibit 100-fold higher estrogen activity than BPA (concentrations of  $10^{-5}$   
63 to  $10^{-10}$  M),<sup>13</sup> while MBP can be 1000-fold more potent (concentrations of  $10^{-5}$  to  $10^{-9}$  M).<sup>14</sup>  
64 Although the *ipso*-substitution pathway of the P450-catalyzed metabolic activation of BPA is most  
65 likely a minor pathway under most circumstances, such strong endocrine-disrupting activity of the  
66 metabolites makes this pathway important to the overall environmental risk assessment, especially  
67 under conditions where glucuronidation is impaired by e.g. other compounds or for genetic or  
68 developmental reasons. For example, human fetal livers show little or no glucuronidation<sup>16</sup> and in  
69 contrast to rodents express significant levels of P450 leading to metabolizing many xenobiotic  
70 compounds even at the prenatal stage.<sup>17,18</sup> thus P450-catalyzed metabolic activation is more likely  
71 relatively more significant in the fetus.<sup>3,19,20</sup>

72 **Scheme 1.** Major Metabolic Pathways of Bisphenol A



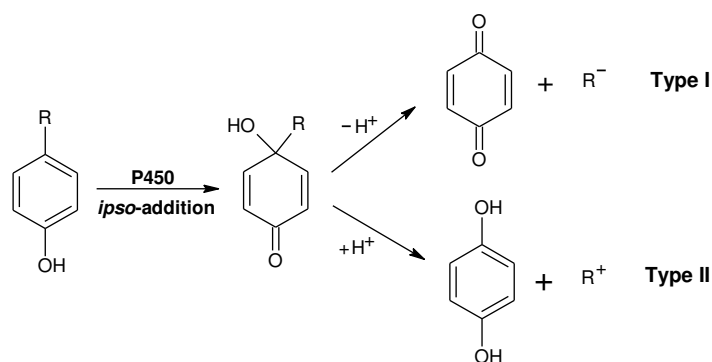
80 Formation of metabolites via *ipso*-substitution constitutes about 20% of the competing *ortho*-  
81 OH-BPA formation via traditional aromatic hydroxylation by P450,<sup>13</sup> i.e. *ipso*-substitution is  
82 quantitatively important in competition with the traditional aromatic hydroxylation of phenolic  
83 EDCs. Oxidation of diverse *p*-substituted phenols by rat liver P450 has been found to result in  
84 elimination of the substituents, including -NO<sub>2</sub>, -CH<sub>2</sub>OH, -COCH<sub>3</sub>, -COPh, -COOH, -F, -Cl, and  
85 -Br.<sup>21</sup> Accordingly, *ipso*-substitution can be categorized into two types depending on the group  
86 eliminated from the quinol intermediate.<sup>21,22</sup> As shown in **Scheme 2**, type I *ipso*-substitution  
87 implies that the substituent eliminates as an anion with formation of a quinone, whereas in type II  
88 *ipso*-substitution the eliminating group is a cation, leading to the formation of a hydroquinone.<sup>21</sup>  
89 However, during oxidation of 4-n-nonylphenol, estrone, estradiol etc. by P450, *ipso*-addition  
90 quinol was formed without C-C bond cleavage.<sup>23,24</sup> Therefore, the *ipso*-substitution, *ipso*-addition,  
91 as well as the above-mentioned aromatic hydroxylation mechanisms compete under various  
92 conditions as relevant pathways, and understanding these mechanisms at the molecular level seems  
93 necessary to access the environmental toxicity and fate of phenolic EDCs. However, the active  
94 species of P450, the iron(IV)-oxo heme cation radical Compound I (Cpd I), responsible for P450-  
95 catalyzed oxidations in all P450 isoenzymes, is short-lived and one of the most potent oxidants in  
96 nature,<sup>25,26</sup> and thus several details of its catalytic action are inaccessible by standard experimental  
97 methods. Specially, two possible pathways for P450-catalyzed *ipso*-substitution via a quinol  
98 intermediate should be distinguished; one involving initial formation of a phenoxy radical and  
99 the other involving the formation of an epoxide via O-addition.<sup>27-29</sup>

100 Analysis of enzyme mechanisms using computational chemistry may identify with semi-  
101 quantitative accuracy the electronic structure features governing reactivity.<sup>30-38</sup> Density functional  
102 theory (DFT) has been used to study many P450-catalyzed oxygenation reactions including

103 hydroxylation of C-H bonds, epoxidation of C=C bonds, oxidation of aromatic rings, oxidation of  
104 heteroatoms etc.<sup>33</sup> The main goal of this work is to show how DFT can be used to elucidate the  
105 full molecular mechanism of the P450-dependent metabolism of phenolic EDCs and to identify  
106 how and when environmentally related *ipso*-substitution, and formation of the very estrogenic  
107 dimer-type metabolites can occur. BPA was used to obtain the full mechanistic picture because of  
108 its prominence in the environment,<sup>39,40</sup> with rich experimental data of its P450-catalyzed  
109 metabolism<sup>13,14</sup> for validation of the computationally obtained mechanisms. The work was  
110 extended to also study the P450-catalyzed biotransformation mechanisms of several other widely-  
111 used phenolic EDCs, such as bisphenol analogues, alkylphenols and chlorophenols. The  
112 fundamental electronic drivers that govern *ipso*-addition vs. *ipso*-substitution and type I vs. type  
113 II substitute elimination were identified, directly relevant for screening P450-catalyzed  
114 biotransformation of many emerging environmental phenolic EDCs.

115

116 **Scheme 2.** Proposed *ipso*-Substitution Mechanisms of P450-Catalyzed Substituent Elimination<sup>a</sup>



117

118 <sup>a</sup> The reactive position is defined as the *ipso*-position; R represents the elimination substituent.

119

120

## 121 **Computational Methodology**

122 **DFT Calculations with Cpd I of P450.** As is common practice,<sup>29,41-43</sup> the six-coordinate tri-  
123 radicaloid ferryl complex  $\text{Fe}^{4+}\text{O}^{2-}(\text{C}_{20}\text{N}_4\text{H}_{12})^{-1}(\text{SH})^{-1}$  was used to model the enzymatic active site  
124 of Cpd I of P450. Cpd I of P450 exists in two close-lying electronic states, a high-spin (HS) quartet  
125 state and a low-spin (LS) doublet state.<sup>33,44</sup> All geometries on both the LS and HS routes were  
126 optimized with unrestricted DFT using the B3LYP hybrid density functional<sup>45,46</sup> in combination  
127 with the LAN2DZ basis set<sup>47</sup> on iron and 6-31G on other atoms (denoted BSI). B3LYP was chosen  
128 because it can reproduce measured kinetic isotope effects for P450-catalyzed reactions,<sup>48</sup> electron  
129 paramagnetic resonance parameters for penta-coordinated heme in P450 enzyme,<sup>49</sup> generate  
130 geometries consistent with crystal structures,<sup>50</sup> and show qualitatively accurate relative energies  
131 vs. benchmark CASSCF calculations.<sup>51</sup> Intrinsic reaction coordinate (IRC) calculations were  
132 performed to verify the rate-determining transition states connecting the reactants and  
133 intermediates on the potential energy surface (**Figure S1-S22** in the Supporting Information).  
134 Please note that the basis-set superposition error (BSSE) has been reported to be very small for  
135 reactant complexes of P450-catalyzed oxidation reactions,<sup>52</sup> but they may affect the relative  
136 energies of very large vs. small substrates and thus we did not include these minor contributions  
137 to the energies in the following as our substrates are similar in size and type.

138 In order to evaluate broadly the sensitivity of the reaction mechanism toward the choice of  
139 density functional, in addition to the B3LYP energies (**Table S1** in the Supporting Information),  
140 we performed unrestricted single-point calculations with other hybrid, local, and non-hybrid  
141 functionals, i.e. TPSSh,<sup>53,54</sup> B3PW91,<sup>46,55</sup> BLYP<sup>45,56</sup> MPW1PW91,<sup>57</sup> and M06L<sup>58</sup> using the  
142 B3LYP/BSI optimized geometries for the P450-catalyzed metabolic mechanisms of BPA (**Table**  
143 **S2** in the Supporting Information). The same qualitative picture was obtained with all of the

144 functionals, and we therefore focused in the following on the B3LYP results. To test the basis set  
145 effect on geometry optimization, the molecular species involved in the initial H-abstraction from  
146 the phenolic group as well as in the O-addition to the aromatic ring of BPA were optimized at the  
147 B3LYP/BSI\*\* level, producing few geometrical and energetic discrepancies as compared with the  
148 results obtained at the B3LYP/BSI level (detailed data in **Table S3** and **Figure S23** in the  
149 Supporting Information). Hence the basis set BSI was used for geometry optimizations throughout  
150 the remaining work.

151 Analytical frequency calculations were used to ensure that there was no imaginary frequency  
152 for any ground state, and only one imaginary frequency for all transition states. The vibrational  
153 frequencies were also used to calculate the zero-point energy (ZPE) and thermal and entropic  
154 corrections to the free energy at 298.15 K and 101.325 kPa. More accurate energies were obtained  
155 using single-point calculations with the SDD<sup>59</sup> basis set on iron and the 6-311++G\*\* basis set for  
156 all other atoms (denoted BSII). Bulk polarity effects were evaluated by the PCM solvation model<sup>60</sup>  
157 using chlorobenzene with a dielectric constant of 5.6 at the B3LYP/BSI level; this dielectric  
158 constant provides a good estimate of the polarization caused by the dipoles of the protein pocket  
159 near the axial cysteine.<sup>61</sup> We also evaluated the bulk polarity effect using the SMD solvation  
160 model<sup>62</sup> for the P450-catalyzed mechanisms of BPA; the H-abstraction and O-addition steps  
161 occurred with only slightly higher energies (**Table S4** in the Supporting Information). In addition,  
162 we evaluated PCM energies using cyclohexane ( $\epsilon=2.0$ ), 1-bromopropane ( $\epsilon=8.0$ ), ethanol ( $\epsilon=24.9$ ),  
163 and acetonitrile ( $\epsilon=35.7$ ). Except for a minor difference in energy for the oxidation of BPA, the  
164 same qualitative picture was obtained throughout (**Table S5** in the Supporting Information).  
165 Dispersion interactions were considered by performing single-point energy calculations with the  
166 B3LYP-D3/BSI level since B3LYP itself does not include dispersion by design.<sup>63</sup> The relative free

167 energies of the P450 oxidation reactions shown below were estimated by combining B3LYP/BSII  
168 single-point energies with PCM solvation and dispersion corrections, as well as Gibbs free energy  
169 corrections from optimizations at the BSI level, unless pointed out specifically.

170 The cluster approach of studying the reaction mechanism treats the catalytic active site of the  
171 enzyme by including key surrounding amino acids and treating all these interactions fully quantum  
172 mechanically.<sup>38</sup> BPA is mainly catalyzed by P450 isoforms 3A4 and 3A5,<sup>13</sup> and therefore we used  
173 the P450 3A4 crystal structure (PDB code: 1W0G)<sup>64</sup> to produce a larger model of the active site.  
174 As shown in **Figure S24** in the Supporting Information, the Cpd I model is the same in the large  
175 and small model, whereas six important second-shell residues, ARG105, ILE301, THR309 and  
176 ALA370 and the peptide chain of ALA305–GLY306 have been included in the large model, with  
177 key central atoms locked in their crystallographic positions to maintain the protein scaffold  
178 packing, steric effects, and hydrogen bond geometries. The large model is charge-neutral and  
179 contains 138 atoms, and the reaction mechanism was investigated for both the HS and LS states.  
180 The geometry optimization, more accurate single-point calculations, evaluation of the bulk polarity  
181 effects, and dispersion interactions were all performed in the same way for both the large and small  
182 models. The results are discussed in detail in the Supporting Information, where all energies are  
183 compiled in **Tables S1-S31**. Importantly, we conclude that the small and large models are in good  
184 agreement on the preferred pathways (**Figure S25** in the Supporting Information), probably  
185 because the main energy effects and electronic reorganizations occur near the iron-oxygen moiety.  
186 We thus performed an extended series of calculations based on the small model as discussed below.

187 **Reaction Energy Calculations for the Decomposition of Quinol Intermediates.** All  
188 geometries for the decomposition reactions of various *ipso*-addition quinol intermediates from  
189 P450-catalyzed *ipso*-position metabolism were optimized at the B3LYP/6-31G\*\* level in water

190 solution ( $\epsilon=78.4$ ) with PCM. Then based on the optimized structures, single-point calculations  
191 were performed in PCM water solution with D3 dispersion corrections at the B3LYP/6-311++G\*\*  
192 level. The reported reaction free energies for decomposition of quinol intermediates are described  
193 by PCM//B3LYP/6-311++G\*\* with water solution and D3 dispersion corrections, as well as free  
194 energy corrections from B3LYP/6-31G\*\* geometry optimizations.

195 All calculations of this work were carried out with the Gaussian 09 D.01 program package.<sup>65</sup>

196

## 197 **Results and Discussion**

### 198 **Reaction Mechanisms of P450-Catalyzed Bisphenol A**

199 **H-abstraction vs. O-addition.** Figure 1 shows two computed competitive reaction  
200 mechanisms of BPA catalyzed by P450, one involving initial H-abstraction from the phenolic  
201 group, and the other involving initial O-addition to the  $\pi$ -system of the aromatic ring. As is  
202 common in P450 reactions,<sup>33</sup> both the HS and LS pathways are available due to the near-degenerate  
203 states of Cpd I. The reactions start from reactant complexes ( ${}^{4,2}\text{RC}$ ), in which the H-atom of the  
204 phenolic group of BPA interacts with the iron-oxo moiety of Cpd I. Then,  ${}^{4,2}\text{RC}$  may go through  
205 H-abstraction transition states  ${}^{4,2}\text{TS}_\text{H}$  with formation of the intermediate complexes ( ${}^{4,2}\text{I}_\text{H}$ )  
206 involving iron-hydroxo species and the phenoxy radical of BPA. The HS transition state  ${}^4\text{TS}_\text{H}$   
207 appears slightly later on the reaction coordinate than its LS counterpart  ${}^2\text{TS}_\text{H}$ , with BPA–O $\cdots$ H  
208 and H $\cdots$ O–Fe distances of 1.211 vs. 1.207 Å and 1.203 vs. 1.212 Å, respectively. These H-  
209 abstraction transition states are characterized by almost linear O $\cdots$ H $\cdots$ O configurations as well as  
210 large imaginary frequencies (HS:  $i1521\text{ cm}^{-1}$ ; LS:  $i1569\text{ cm}^{-1}$ ). Cpd I is a potent H-atom abstractor  
211 toward the phenolic group, with a H-abstraction barrier of only 0.4/0.3 kcal/mol for the HS/LS  
212 state, similar to the minor H-abstraction barriers obtained for the phenolic group of paracetamol<sup>29</sup>

213 and the amino group of anilines<sup>42</sup>, yet much lower than the H-abstraction barriers obtained from  
 214 C–H hydroxylation.<sup>41,52,66</sup> In addition, the formed complex intermediates (<sup>4,2</sup>I<sub>H</sub>) are stable, with  
 215 exothermic reaction energies of -8.0/-7.4 kcal/mol for the HS/LS state. Note that dispersion effects  
 216 lower the H-abstraction barriers by a substantial 2.5 kcal/mol, a magnitude consistent with  
 217 previous findings for P450 reactions.<sup>67</sup>

218 Another possible reaction path starting from <sup>4,2</sup>RC is the addition of the oxo group of Cpd I  
 219 onto the unsubstituted aromatic ring of BPA via C-O bond-forming transition states <sup>4,2</sup>TS<sub>O</sub>, which  
 220 produce tetrahedral intermediates. As shown in **Figure 1**, compared with the LS species, TS<sub>O</sub> in  
 221 the HS state is more advanced (shorter O···C bond) with a higher degree of aromatic activation.  
 222 The calculated barriers for O-addition at the *ortho*-position (<sup>4,2</sup>TS<sub>Oo</sub>) and *meta*-position (<sup>4,2</sup>TS<sub>Om</sub>)  
 223 are 17.5/14.5 and 19.9/17.1 kcal/mol, respectively, on the HS/LS state surfaces. Comparison of  
 224 the barriers of the H-abstraction and O-addition steps shows clearly that the H-abstraction reaction  
 225 is much more favorable. Therefore, we focused on the H-abstraction pathway in the following  
 226 sections.

227

228

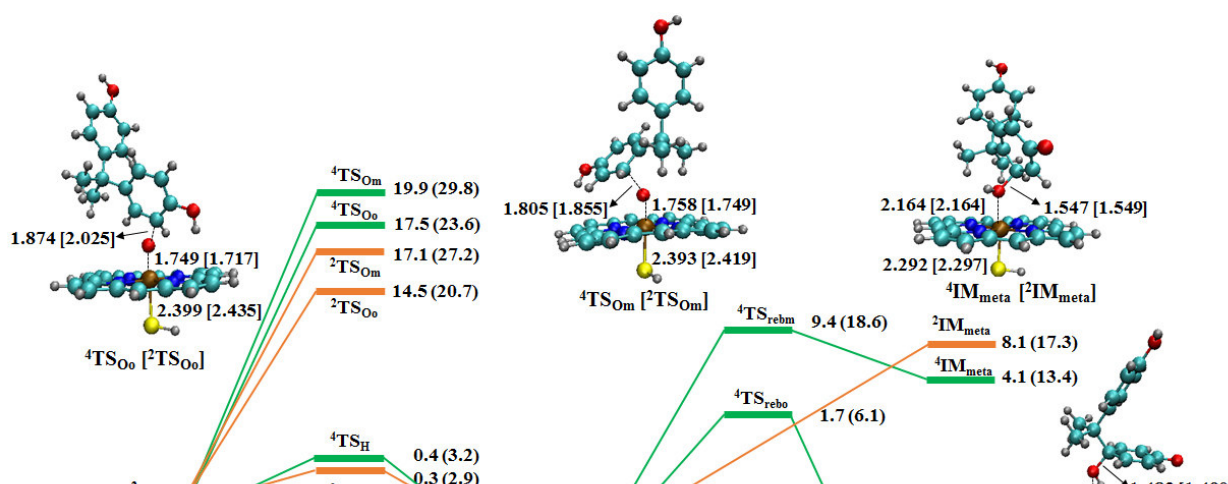
229

230

231

232

233



234  
235  
236  
237  
238  
239  
240  
241  
242

243 **Figure 1.** Free energy profile of BPA catalyzed by Cpd I of P450, along with the optimized  
244 geometries of the key reaction species in the HS and LS states. Free energies (kcal/mol) are relative  
245 to the quartet reactant complex  ${}^4\text{RC}$  at the B3LYP/BSII//BSI level including solvation ( $\epsilon=5.6$ ) and  
246 dispersion corrections (no parentheses), and without dispersion (in parentheses). Geometrical  
247 parameters (lengths in Å and angles in degrees) are shown as the HS [LS] state.

248

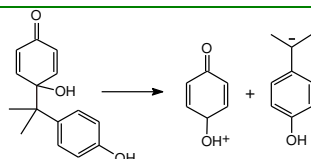
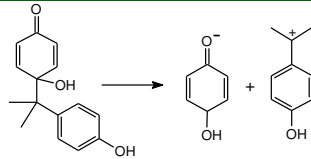
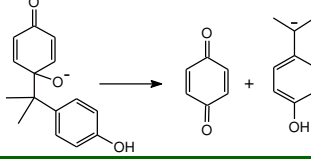
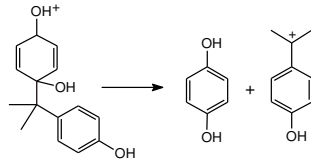
249 **OH Radical Rebound Mechanism.** For the H-abstraction pathway, formation of the  
250 intermediate complex ( ${}^{4,2}\text{IM}_\text{H}$ ) is followed by rebound of the phenoxy radical onto the iron-  
251 hydroxo species. This occurs via formation of covalent bonds at the *ipso*-, *ortho*- or *meta*-carbon  
252 of the aromatic ring of BPA to yield corresponding addition quinol intermediates  $\text{IM}_\text{ipso}$ ,  $\text{IM}_\text{ortho}$  or  
253  $\text{IM}_\text{meta}$ . As shown in **Figure 1**, all the rebound steps are essentially barrierless in the LS state, while  
254 they proceed with significant barriers of 7.8-17.4 kcal/mol on the HS surface. The rebound  
255 reactions at the *ipso*- and *ortho*-carbon are exothermic for both the HS and LS pathways, with  
256 reaction energies of -31.6/-29.5 and -30.3/-32.7 kcal/mol, respectively, while the rebound reactions

257 at the *meta*-carbon are endothermic (+4.1/+8.1 kcal/mol). Importantly, the thermodynamically  
258 unfavorable rebound reactions associated with this mechanism can explain the lack of  
259 experimental detection of the hydroxylation product of the *meta*-position during P450-dependent  
260 metabolism of BPA.<sup>13</sup> Note that the HS rebound barriers are significantly larger than the initial H-  
261 abstraction barriers, implying that <sup>4</sup>Cpd I is a sluggish oxidant and unlikely to play a key role.  
262 Thus, OH recombination with the phenyl ring of BPA only occurs via the LS potential energy  
263 surface. Accordingly, OH radical rebound will proceed under thermodynamic control, and the  
264 reaction energy difference between formation of IM<sub>ortho</sub> of -32.7 kcal/mol and IM<sub>ipso</sub> of -29.5  
265 kcal/mol for the LS state of about 3.2 kcal/mol, favors IM<sub>ortho</sub> formation but also translates into a  
266 lower fraction of IM<sub>ipso</sub> formed. This is in accordance with the observation that metabolites formed  
267 via *ipso*-substitution constitute approximately 20% of the products of the traditional aromatic  
268 hydroxylation pathway of P450.<sup>13</sup>

269 **Decomposition Reaction of the Quinol Intermediate (IM<sub>ipso</sub>) of BPA.** Hydroquinone,  
270 isopropenylphenol (IPP), and hydroxycumyl alcohol (HCA) were detected as metabolites upon C-  
271 C bond scission via *ipso*-substitution in experiments of the P450-catalyzed degradation of  
272 BPA,<sup>13,68</sup> which means that the *ipso*-metabolism reaction of BPA does not stop in the quinol form.  
273 In order to understand the complete mechanistic picture, we need to establish the nature of the  
274 quinol intermediate decomposition. As mentioned above, there are two types of substituent  
275 elimination from the quinol intermediate. While hydroquinone has been detected in the  
276 experiments of oxidation of BPA by P450,<sup>13,68-70</sup> quinone is also easily transformed to  
277 hydroquinone upon NADPH-induced reduction in rat liver microsomes.<sup>21</sup> Therefore, it is difficult  
278 to conclude whether the decomposition of the *ipso*-addition quinol intermediate (IM<sub>ipso</sub>) proceeds  
279 via type I or type II elimination based on the available experimental data.

280

281 **Table 1.** Computed Aqueous-Phase Free Energies ( $\Delta G$ ) (kcal/mol) for the Decomposition  
 282 Reactions of Quinol of BPA

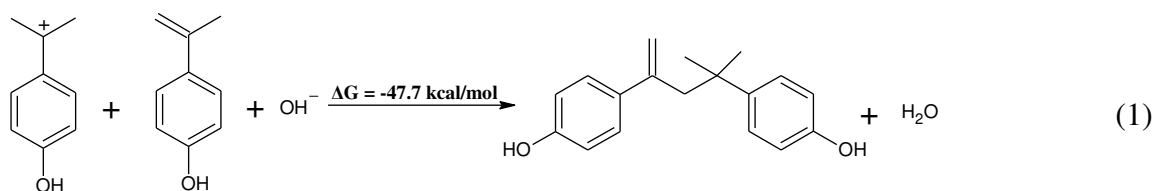
Condition	Elimination Type	$\Delta G$ (kcal/mol)	
Neutralization	Type I		82.1
Neutralization	Type II		11.1
Deprotonation	Type I		21.8
Protonation	Type II		-30.7

283

284 As shown in **Table 1**, the heterolytic decomposition of  $IM_{ipso}$  may proceed charge-neutrally  
 285 or after protonation or deprotonation in water solution. The computations suggest that the charge-  
 286 neutral decompositions of  $IM_{ipso}$  leading to a carbocation (type II *ipso*-substitution) or carbanion  
 287 intermediate (type I *ipso*-substitution) have reaction energies of +11.1 kcal/mol and +82.1 kcal/mol,  
 288 respectively. The decomposition of  $IM_{ipso}$  after deprotonation (type I *ipso*-substitution) is  
 289 endothermic by +21.8 kcal/mol. Thus, the most feasible pathway is decomposition after  
 290 protonation with production of the carbocationic intermediate and hydroquinone (type II *ipso*-  
 291 substitution) with a reaction energy of -30.7 kcal/mol, which supports that the quinol intermediate  
 292 generated in the P450 enzyme pocket can readily dissociate from the pocket and decompose in a  
 293 nonenzymatic environment after protonation.

294 The carbocationic intermediate can react to produce IPP by fast proton transfer to a hydroxyl  
295 ion with a reaction energy of -48.7 kcal/mol, or into HCA by absorbing the hydroxyl ion with a  
296 reaction energy of -44.0 kcal/mol (using the same method of calculations as for the decomposition  
297 of quinols). This mechanism would explain the puzzling observation that no quinol of BPA has  
298 ever been detected as an *ipso*-addition metabolite:<sup>13,68-70</sup> From our reaction diagrams, it is an  
299 unstable intermediate that quickly collapses to the product.

300 **MBP Formation.** A dimer-type metabolite MBP has been shown to exhibit the highest  
301 estrogen activity among all BPA metabolites, and thus we investigated also the MBP formation  
302 mechanism. First, we examined the feasibility of the previously suggested radical pathway of  
303 MBP formation; this reaction occurs between the isopropenylphenol radical formed by oxidative  
304 cleavage of the carbon–phenyl bond, and IPP, as supported by the disappearance of the mass peak  
305 of MBP when a radical scavenger was added to the incubation system.<sup>14</sup> However, as shown in  
306 **Table S31** in the Supporting Information, the cleavage reactions of the carbon–phenyl bond of  
307 BPA and the phenoxy radical of BPA in the enzymatic environment are both highly endothermic,  
308 and thus the radical pathway seems unfavorable. According to LC/MS/MS investigation, the  
309 metabolite of BPA gave a negative mass peak at  $[M-H]^-$  267 in LC/MS and a single daughter ion  
310 at  $m/z$  133 on MS/MS analysis, corresponding to MBP and IPP, respectively.<sup>14</sup> Alternatively, the  
311 dimer-type structure of MBP triggers cationic polymerization, by which the carbocation reacts  
312 with IPP, with both reactants originating from the *ipso*-substitution pathway, initiating  
313 polymerization and generation of MBP, as shown in eq 1:



315 The obtained reaction energy of  $-47.7$  kcal/mol provides a notable driving force for this cationic  
316 polymerization pathway to form MBP (using the same method of calculation as for the  
317 decomposition of quinols). The P450-catalyzed *ipso*-substitution suggested above proceeds  
318 through the radical pathway involving H-abstraction from BPA to produce a phenoxy radical,  
319 which would explain why adding a radical scavenger to the incubation system prevents MBP  
320 formation during the experiment.

321

## 322 **The Reaction Patterns of P450-Catalyzed *ipso*-Position Metabolism**

### 323 **Initial Rate-Determining Step for the Production of *ipso*-Addition Quinol Intermediates.**

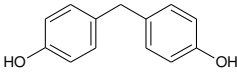
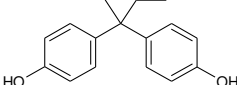
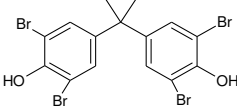
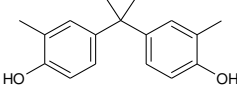
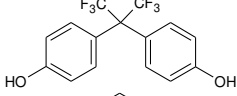
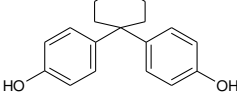
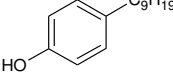
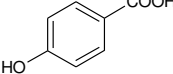
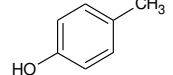
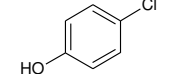
324 In order to study the detailed reaction mechanism and to verify the initial rate-determining step for  
325 *ipso*-position metabolism, we studied several other widely-used phenolic EDCs distributed in the  
326 environment such as bisphenol analogues, alkylphenols and chlorophenols with available *in vitro*  
327 or *in vivo* assay data on the P450 metabolism.<sup>3,14,15,21,23,71</sup> As shown in **Table 2**, these phenolic  
328 EDCs include bisphenol F (BPF), bisphenol B (BPB), tetrabromobisphenol A (TBBPA),  
329 dimethylbisphenol A (DMBPA), bisphenol AF (BPAF), bisphenol Z (BPZ), 4-n-nonylphenol  
330 (NP1), *p*-hydroxybenzoic acid (PHBA), *p*-cresol (PC), and *p*-chlorophenol (PCP). The relative  
331 energies of the H-abstraction from the phenolic group as well as O-addition at the aromatic *ortho*-  
332 carbon position on the LS potential energy surface are listed in **Table 2**. The barriers of H-  
333 abstraction (0.4-3.1 kcal/mol) are much lower than that for O-addition (14.2-21.0 kcal/mol) for all  
334 phenolic EDCs, i.e. the initial step involves H-abstraction by Cpd I from the phenolic group  
335 leading to an intermediate complex consisting of an iron-hydroxo group and a phenoxy radical.  
336 Within the intermediate complex, as in the reaction of BPA catalyzed by P450, the OH rebounds  
337 onto both the *ipso*- and *ortho*-carbon to form the hydroxylation intermediates with markedly

338 exothermic reaction energies (-36.3 to -16.5 kcal/mol). The OH rebound barriers for the HS  
339 pathway (4.4-13.5 kcal/mol) are much higher than the initial H-abstraction barriers (see details in  
340 **Table S9** in the Supporting Information), while the OH rebound on the LS pathway is essentially  
341 barrier-free. Therefore, we suggest that the P450-catalyzed *ipso*-position metabolism of these  
342 diverse phenolic EDCs follows the same reaction mode as displayed in **Figure 1** of BPA, i.e. via  
343 H-abstraction followed by an essentially barrierless OH rebound onto the *ipso*-carbon to produce  
344 the corresponding *ipso*-addition quinol intermediate mainly via the LS state.

345 As shown in **Table 2**, compared with the thermodynamic data on OH rebound onto the *ortho*-  
346 positions, the rebound reactions onto the *ipso*-positions are 2.3 and 2.6 kcal/mol more favorable  
347 for PCP and NP1, respectively, but 0.7-9.1 kcal/mol less favorable for all other phenolic EDCs.  
348 Although the driving force for *ortho*-addition relative to *ipso*-addition is much larger for PBHA,  
349 BPAF and TBBPA, the obtained energy difference of 6-9 kcal/mol may still translate into a lower  
350 fraction of the *ipso*-addition quinol intermediates. Regardless of the external factors, we conclude  
351 that the P450-catalyzed *ipso*-position metabolism competes with *ortho*-position metabolism in the  
352 LS state under thermodynamic control. This is consistent with the experiments, in which *ipso*-  
353 substitution/addition metabolites of all studied phenolic EDCs studied in this work were observed  
354 in the presence of P450, such as 4-hexafluorohydroxyisopropylidene-phenol from BPAF, and 2,6-  
355 dibromo-4-(2-hydroxypropane-2-yl) phenol from TBBPA, which may be produced by the addition  
356 of hydroxyl ion to the carbocations as the *ipso*-substitution products, as well as 4-nonyl-4-hydroxy-  
357 cyclohexa-2,5-dienone produced from 4-NP1 as the *ipso*-addition product. Until now, there are no  
358 reported ratios of *ipso*-addition vs. *ortho*-addition products for most phenolic EDCs. However, the  
359 calculated energy difference between *ipso*-addition and *ortho*-addition can be used as a probe for  
360 predicting the relative importance of these two pathways.

361

362 **Table 2.** Relative Free Energies (kcal/mol) for P450-catalyzed *ipso*-Position Metabolism of  
 363 Phenolic EDCs via the LS state

Phenolic EDCs		<sup>2</sup> TS <sub>H</sub>	<sup>2</sup> TS <sub>O<sub>o</sub></sub>	<sup>2</sup> IM <sub>H</sub>	<sup>2</sup> IM <sub>ipso</sub>	<sup>2</sup> IM <sub>ortho</sub>	ΔG <sub>gap</sub>
<b>Bisphenol Analogues</b>	<b>BPF</b> 	2.1	16.6	-6.6	-32.3	-33.0	0.7
	<b>BPB</b> 	1.2	14.2	-6.5	-30.5	-34.1	3.6
	<b>TBBPA</b> 	0.4	19.9	-6.7	-30.1	-36.3	6.2
	<b>DMBPA</b> 	0.4	15.4	-7.8	-30.3	-33.7	3.4
	<b>BPAF</b> 	3.1	19.5	0.6	-17.0	-26.1	9.1
	<b>BPZ</b> 	1.8	16.1	-6.0	-29.0	-32.3	3.3
<b>Alkylphenols</b>	<b>NP1</b> 	1.6	18.2	-5.9	-32.4	-29.8	-2.6
	<b>PHBA</b> 	3.0	21.0	1.6	-16.5	-23.6	7.1
	<b>PC</b> 	2.7	17.8	-6.8	-28.8	-30.6	1.8
<b>Chlorophenols</b>	<b>PCP</b> 	2.8	20.1	-2.9	-29.0	-26.7	-2.3

364

365 **Decomposition Reaction Mechanisms of Diverse Quinol Intermediates.** Experimental  
 366 work on P450-catalyzed phenolic EDCs has shown that *ipso*-substitution prior to *ipso*-addition  
 367 does not always occur.<sup>21,23,24,69</sup> However, the reason why some phenolic EDCs are stopped at the  
 368 *ipso*-addition step is unknown. It is also difficult to determine which type of elimination (type I or  
 369 type II) occurs during *ipso*-substitution due to the complex biological redox environment. We  
 370 focused on the decomposition mechanisms of the diverse *ipso*-addition quinol intermediates

371 derived from the diverse phenolic EDCs described above with the available experimental  
372 information,<sup>21,69</sup> but excluded TBBPA and BPZ, for which our attempts to locate the quinol  
373 intermediates after protonation give fragmental type II products directly. The thermodynamic data  
374 for the decomposition of quinol intermediates in all possible pathways were evaluated and the most  
375 favorable decomposition paths via type II and type I *ipso*-substitution are shown in **Figure 2**.

376  
377  
378  
379  
380  
381  
382  
383  
384  
385  
386  
387  
388  
389  
390  
391  
392  
393  
394  
395  
396  
397  
398  
399

400 **Figure 2.** Computed free energies (kcal/mol) for the decomposition reactions of diverse *ipso*-  
401 addition quinols along the favorable pathways: (left) type II substitution with the hydride ion  
402 affinity (HIA, kcal/mol) of the formed carbocation; (right) type I substitution. <sup>a</sup> R represents the  
403 elimination substituent.

404  
405 As shown in **Figure 2**, for all bisphenol analogues and alkylphenols except for PHBA, the  
406 decomposition of the formed *ipso*-addition quinols after protonation with formation of carbocation  
407 and hydroquinone (type II substitution) is the most favorable pathway. The decomposition

408 reactions for the *ipso*-addition quinols from PC and NP1 are distinctly endothermic, which is fully  
409 in line with experimental observations of the P450-catalyzed conversion of these two alkylphenols  
410 showing only *ipso*-addition quinols were produced without detecting any *ipso*-substitution  
411 products.<sup>21,23,69</sup> However, for other bisphenol analogues and alkylphenols, the decomposition of  
412 the formed *ipso*-addition quinols after protonation can proceed, leading to C-C bond cleavage with  
413 significant exothermic energies. It is found that the P450-catalyzed *ipso*-substitution products are  
414 obtained from the *ipso*-addition quinols when the carbon at the benzylic position contains one or  
415 more alkyl branches. More alkyl branches stabilize the carbocation via inductive and  
416 hyperconjugative effects; this results in the spontaneous decomposition of the formed *ipso*-  
417 addition quinols after protonation. The hydride ion affinity (HIA) can be used for comparing the  
418 carbocation stability of dissimilar structures directly, defined according to eq (2):<sup>72</sup>



420 The HIA obtained at the B3LYP/6-311++G\*\* level using frequency analysis at 298.15 K and 1  
421 atm pressure are listed in the lower left of **Figure 2**. The experimental HIA is available for CH<sub>3</sub><sup>+</sup>  
422 (312 kcal/mol),<sup>72</sup> the same as the computed HIA of 312 kcal/mol, which supports the reliability of  
423 the computational method. The reaction free energies of decomposition of the quinol intermediates  
424 generally increase with increasing HIA of the formed carbocations ( $r^2 = 0.95$ ,  $\Delta\text{G} = 1.4\text{HIA} +$   
425 245.5). This pattern indicates that the HIA values are useful for preliminary evaluation of the  
426 decomposition free energies of the *ipso*-addition quinols produced from bisphenol analogues and  
427 alkylphenols with associated formation of a carbocation and a hydroquinone (type II substitution).

428 For quinol intermediates with electronegative substituents, such as -Cl and -COOH, as shown  
429 in **Figure 2**, there are two possible pathways for substituent elimination from quinol with the  
430 formation of an anion and a quinone (type I *ipso*-substitution): 1) elimination of the substituent

431 after deprotonation with the formation of an anion and quinone; 2) involving the prior intra-  
432 molecular H-arrangement from OH to the electronegative substituents to produce the  
433 corresponding inorganic acid and quinone neutrally. The charge-neutral intra-molecular H-  
434 arrangement pathway with formation of the inorganic acid and quinone is more favorable for  
435 decomposition of quinol intermediates with electronegative substituents; in this case the inorganic  
436 acid can dissociate into an anion. The pathway we have obtained for type I *ipso*-substitution  
437 extends the formal definition of type I *ipso*-substitution in P450 chemistry. In particular, the  
438 elimination of -COOH from quinol after deprotonation is not feasible because it is endothermic,  
439 while the exothermic elimination of -COOH during the intra-molecular H-arrangement route is  
440 favorable. This is in accordance with the experimental observation that PHBA can be subject to  
441 *ipso*-substitution when the reaction is catalyzed by P450.<sup>21</sup>

## 442 443 **Environmental Implications**

444 Identification of EDCs is one of the most important goals of environmental chemical hazard  
445 screening, which has come a long way in developing useful test assays and mechanism-based  
446 screening techniques.<sup>10</sup> Many synthetic compounds released into the environment may be readily  
447 transformed, especially by P450 enzymes, into metabolites exhibiting much higher endocrine-  
448 disrupting activity than their parent compounds. Knowledge of detailed metabolic mechanisms  
449 gives insight into the bioactivation. Accordingly, it is critical in environmental risk assessment to  
450 understand metabolic pathways and to have effective tools for predicting the fate of metabolites.  
451 Methods that analyze and predict the metabolic fate of molecules thrive within the field of  
452 medicinal chemistry,<sup>73</sup> but not so much within environmental sciences despite the similarity of  
453 involved tools. In medicinal chemistry, many drugs require P450-mediated bioactivation to elicit  
454 their pharmacological effect via metabolites that can be characterized in relatively high

455 concentrations. In contrast, environmental pollutants such as EDCs and their metabolites normally  
456 occur in trace amounts while still important at these levels, and thus identification of their  
457 biotransformation products seems more difficult, and mechanism-based methods to provide  
458 putative metabolites efficiently are of interest. Experimental methods often require expensive  
459 equipment, expertise, running costs and time, which may reduce their applicability when screening  
460 large libraries of compounds. Thus, there is substantial interest in the development of fast, accurate  
461 computational tools that can predict metabolism with higher throughput and lower cost. These  
462 computational tools should: (i) predict the site of metabolism and (ii) predict the metabolite  
463 structure from these sites.<sup>74</sup>

464 The present work shows how detailed DFT investigations of metabolic pathways can  
465 rationalize the formation of metabolites resulting from the P450-catalyzed reactions of diverse  
466 environmental phenolic EDCs such as bisphenol analogues, alkylphenols and chlorophenols,  
467 thereby achieving these two tasks, as particularly emphasized for one of the prominent phenolic  
468 EDCs, BPA. The barrier for the most favorable H-abstraction/OH-rebound mechanism involving  
469 both the *ipso*- and *ortho*-position hydroxylation is one of the lowest reported barriers, as far as we  
470 know. The H-abstraction/OH-rebound reaction with formation of the quinol intermediate seems to  
471 be a general reaction mechanism for phenolic EDCs, as shown by studying a diverse group of such  
472 compounds in this work. In case of the *ipso*-addition quinol intermediate, we can distinguish type  
473 II vs. type I *ipso*-substitutions based on thermodynamic data, and *ipso*-substitution vs. *ipso*-  
474 addition based on the stability of the eliminating carbocation by both qualitative and quantitative  
475 analysis. Notably, the formation mechanism of the highly estrogenic metabolites HCA and dimer-  
476 type MBP, which arises from oxidation of BPA catalyzed by P450, has been revealed in detail.  
477 Our results show that both metabolites originate from a carbocationic intermediate produced in the

478 *ipso*-substitution pathway. This pathway gives insight into the potentially important bioactivation  
479 of many other alternatives to BPA whose metabolic mechanisms remain unidentified, in particular  
480 under conditions where P450-catalyzed metabolism is important relative to glucuronidation (e.g.  
481 if this pathway is inhibited or genetically or otherwise down-regulated, e.g. in the fetus). However,  
482 even when non-P450 pathways dominates by 10-, 100- or even 1000-fold, the *ipso*-position  
483 metabolites may still contribute to toxicity due to their correspondingly higher potency.

484 The hydroxylated metabolites of many emerging phenolic pollutants, such as OH-PBDEs and  
485 OH-PCBs, have been reported to be even stronger EDCs than their precursors,<sup>75,76</sup> and based on  
486 their similar molecular structures we speculate that they may involve products from the *ipso*-  
487 substitution/addition pathway catalyzed by P450, which has thus far largely been neglected.  
488 Recently, the biotransformation of sulfonamide antibiotics in the environment has been reported  
489 to proceed via the *ipso*-substitution pathway.<sup>77</sup> Therefore, *ipso*-substitution seems to be a much  
490 more common and, even at low turnover, more important toxification pathway than previously  
491 thought for a wide variety of persistent pollutants. Our study has identified the detailed electronic  
492 structure changes and transition states probably involved in these processes, as well as provided  
493 simple tools for determining the relative importance of these pathways based on thermodynamic  
494 considerations that we envision will be valuable for determining the environmental toxicity and  
495 fate of emerging phenolic EDCs.

496

## 497 **ASSOCIATED CONTENT**

498 **Supporting Information.** Full citation for reference 73; Energies for all molecular species;  
499 Intrinsic reaction coordinate (IRC) for verifying transition states; Optimized geometries at the

500 B3LYP/BSI\*\* level of theory; Quantum chemical cluster calculations; Cartesian coordinates of  
501 all structures. This material is available free of charge via the Internet at <http://pubs.acs.org>.

502 **Corresponding Author**

503 \*(L.J.) E-mail: [jilienv@zju.edu.cn](mailto:jilienv@zju.edu.cn)

504 \*(K.P.K.) E-mail: [kpj@kemi.dtu.dk](mailto:kpj@kemi.dtu.dk)

505 **Notes**

506 The authors declare no competing financial interest.

507

508 **ACKNOWLEDGMENT**

509 This work was supported by the National Natural Science Foundation of China (21677125). The  
510 China National Supercomputing Center in Shenzhen and UFZ in Leipzig are acknowledged for  
511 providing the Gaussian 09 package and the high-performance computing clusters. We also thank  
512 the general agreement on cooperation between UFZ Germany and Zhejiang University China (No.  
513 RA-127/13) to give Dr. Li Ji a guest scientist status in UFZ between 2013 and 2015 to have access  
514 to the computing clusters of UFZ.

515

516 **REFERENCES**

517 (1) Gaines, T. B.; Hayes, W. J.; Linder, R. E. Liver metabolism of anticholinesterase compounds  
518 in live rats: Relation to toxicity. *Nature* **1966**, *209*, (5018), 88-89.

519 (2) Ashrap, P.; Zheng, G. M.; Wan, Y.; Li, T.; Hu, W. X.; Li, W. J.; Zhang, H.; Zhang, Z. B.;  
520 Hu, J. Y. Discovery of a widespread metabolic pathway within and among phenolic xenobiotics.  
521 *Proc. Natl. Acad. Sci. U. S. A.* **2017**, *114*, (23), 6062-6067.

522 (3) Chen, D.; Kannan, K.; Tan, H.; Zheng, Z.; Feng, Y. L.; Wu, Y.; Widelka, M. Bisphenol  
523 analogues other than BPA: environmental occurrence, human exposure, and toxicity-a review.  
524 *Environ. Sci. Technol.* **2016**, *50*, (11), 5438-5453.

525 (4) Reinen, J.; Vermeulen, N. P. Biotransformation of endocrine disrupting compounds by  
526 selected phase I and phase II enzymes--formation of estrogenic and chemically reactive  
527 metabolites by cytochromes P450 and sulfotransferases. *Curr. Med. Chem.* **2015**, *22*, (4), 500-527.

528 (5) Guengerich, F. P. Common and uncommon cytochrome P450 reactions related to metabolism  
529 and chemical toxicity. *Chem. Res. Toxicol.* **2001**, *14*, (6), 611-650.

530 (6) Guengerich, F. P. Cytochrome P450 and chemical toxicology. *Chem. Res. Toxicol.* **2008**, *21*,  
531 (1), 70-83.

532 (7) Ribalta, C.; Sole, M. *In vitro* interaction of emerging contaminants with the cytochrome P450  
533 system of Mediterranean deep-sea fish. *Environ. Sci. Technol.* **2014**, *48*, (20), 12327-12335.

534 (8) Yoo, J.; Hirano, M.; Mizukawa, H.; Nomiyama, K.; Agusa, T.; Kim, E. Y.; Tanabe, S.; Iwata,  
535 H. *In vitro* and *in silico* analyses for predicting hepatic cytochrome P450-dependent metabolic  
536 potencies of polychlorinated biphenyls in the Baikal seal. *Environ. Sci. Technol.* **2015**, *49*, (24),  
537 14588-14596.

- 538 (9) Fu, Z. Q.; Wang, Y.; Chen, J. W.; Wang, Z. Y.; Wang, X. B. How PBDEs are transformed  
539 into dihydroxylated and dioxin metabolites catalyzed by the active center of cytochrome P450s: a  
540 DFT study. *Environ. Sci. Technol.* **2016**, *50*, (15), 8155-8163.
- 541 (10) Khetan, S. K. *Endocrine Disruptors in the Environment*. John Wiley & Sons, Inc.: Hoboken,  
542 New Jersey, 2014.
- 543 (11) Welshons, W. V.; Nagel, S. C.; vom Saal, F. S. Large effects from small exposures. III.  
544 Endocrine mechanisms mediating effects of bisphenol A at levels of human exposure.  
545 *Endocrinology* **2006**, *147*, (6 Suppl), S56-69.
- 546 (12) Quesnot, N.; Bucher, S.; Fromenty, B.; Robin, M. A. Modulation of metabolizing enzymes  
547 by bisphenol a in human and animal models. *Chem. Res. Toxicol.* **2014**, *27*, (9), 1463-1473.
- 548 (13) Nakamura, S.; Tezuka, Y.; Ushiyama, A.; Kawashima, C.; Kitagawara, Y.; Takahashi, K.;  
549 Ohta, S.; Mashino, T. *Ips*o substitution of bisphenol A catalyzed by microsomal cytochrome P450  
550 and enhancement of estrogenic activity. *Toxicol. Lett.* **2011**, *203*, (1), 92-95.
- 551 (14) Yoshihara, S.; Mizutare, T.; Makishima, M.; Suzuki, N.; Fujimoto, N.; Igarashi, K.; Ohta,  
552 S. Potent estrogenic metabolites of bisphenol A and bisphenol B formed by rat liver S9 fraction:  
553 their structures and estrogenic potency. *Toxicol. Sci.* **2004**, *78*, (1), 50-59.
- 554 (15) Gramec Skledar, D.; Peterlin Masic, L. Bisphenol A and its analogs: Do their metabolites  
555 have endocrine activity? *Environ. Toxicol. Pharmacol.* **2016**, *47*, 182-199.
- 556 (16) Pacifici, G. M.; Kubrich, M.; Giuliani, L.; de Vries, M.; Rane, A. Sulphation and  
557 glucuronidation of ritodrine in human foetal and adult tissues. *Eur. J. Clin. Pharmacol.* **1993**, *44*,  
558 (3), 259-264.

559 (17) Hakkola, J.; Pelkonen, O.; Pasanen, M.; Raunio, H. Xenobiotic-metabolizing cytochrome  
560 P450 enzymes in the human feto-placental unit: role in intrauterine toxicity. *Crit. Rev. Toxicol.*  
561 **1998**, *28*, (1), 35-72.

562 (18) Hakkola, J.; Raunio, H.; Purkunen, R.; Saarikoski, S.; Vahakangas, K.; Pelkonen, O.;  
563 Edwards, R. J.; Boobis, A. R.; Pasanen, M. Cytochrome P450 3A expression in the human fetal  
564 liver: evidence that CYP3A5 is expressed in only a limited number of fetal livers. *Biol. Neonate*  
565 **2001**, *80*, (3), 193-201.

566 (19) Nahar, M. S.; Liao, C.; Kannan, K.; Dolinoy, D. C. Fetal liver bisphenol A concentrations  
567 and biotransformation gene expression reveal variable exposure and altered capacity for  
568 metabolism in humans. *J. Biochem. Mol. Toxicol.* **2013**, *27*, (2), 116-123.

569 (20) Nahar, M. S.; Liao, C.; Kannan, K.; Harris, C.; Dolinoy, D. C. In utero bisphenol A  
570 concentration, metabolism, and global DNA methylation across matched placenta, kidney, and  
571 liver in the human fetus. *Chemosphere* **2015**, *124*, 54-60.

572 (21) Ohe, T.; Mashino, T.; Hirobe, M. Substituent elimination from *p*-substituted phenols by  
573 cytochrome P450. *ipso*-Substitution by the oxygen atom of the active species. *Drug Metab. Dispos.*  
574 **1997**, *25*, (1), 116-122.

575 (22) Ricken, B.; Kolvenbach, B. A.; Corvini, P. F. *Ips*o-substitution--the hidden gate to  
576 xenobiotic degradation pathways. *Curr. Opin. Biotechnol.* **2015**, *33*, 220-227.

577 (23) Tezuka, Y.; Takahashi, K.; Suzuki, T.; Kitamura, S.; Ohta, S.; Nakamura, S.; Mashino, T.  
578 Novel metabolic pathways of *p*-*n*-nonylphenol catalyzed by cytochrome p450 and estrogen  
579 receptor binding activity of new metabolites. *J. Health Sci.* **2007**, *53*, (5), 552-561.

- 580 (24) Ohe, T.; Hirobe, M.; Mashino, T. Novel metabolic pathway of estrone and 17beta-estradiol  
581 catalyzed by cytochrome P-450. *Drug Metab. Dispos.* **2000**, *28*, (2), 110-112.
- 582 (25) Rittle, J.; Green, M. T. Cytochrome P450 Compound I: capture, characterization, and C-H  
583 bond activation kinetics. *Science* **2010**, *330*, (6006), 933-937.
- 584 (26) Yosca, T. H.; Ledray, A. P.; Ngo, J.; Green, M. T. A new look at the role of thiolate ligation  
585 in cytochrome P450. *J. Biol. Inorg. Chem.* **2017**, *22*, (2-3), 209-220.
- 586 (27) Ortiz de Montellano, P. R.; De Voss, J. J. In *Cytochrome P450: Structure, Mechanism, and*  
587 *Biochemistry*, 3rd ed.; Ortiz de Montellano, P. R., Ed. Kluwer Academic/Plenum Publishers: New  
588 York, 2005; pp 183-230.
- 589 (28) Schyman, P.; Lai, W.; Chen, H.; Wang, Y.; Shaik, S. The directive of the protein: how does  
590 cytochrome P450 select the mechanism of dopamine formation? *J. Am. Chem. Soc.* **2011**, *133*,  
591 (20), 7977-7984.
- 592 (29) Ji, L.; Schuurmann, G. Computational biotransformation profile of paracetamol catalyzed  
593 by cytochrome P450. *Chem. Res. Toxicol.* **2015**, *28*, (4), 585-596.
- 594 (30) Paneth, P. Chlorine kinetic isotope effects on enzymatic dehalogenations. *Acc. Chem. Res.*  
595 **2003**, *36*, (2), 120-126.
- 596 (31) Dybala-Defratyka, A.; Szatkowski, L.; Kaminski, R.; Wujec, M.; Siwek, A.; Paneth, P.  
597 Kinetic isotope effects on dehalogenations at an aromatic carbon. *Environ. Sci. Technol.* **2008**, *42*,  
598 (21), 7744-7750.
- 599 (32) Jensen, K. P.; Ryde, U. Cobalamins uncovered by modern electronic structure calculations.  
600 *Coord. Chem. Rev.* **2009**, *253*, (5-6), 769-778.

- 601 (33) Shaik, S.; Cohen, S.; Wang, Y.; Chen, H.; Kumar, D.; Thiel, W. P450 enzymes: their  
602 structure, reactivity, and selectivity-modeled by QM/MM calculations. *Chem. Rev.* **2010**, *110*, (2),  
603 949-1017.
- 604 (34) Garcia-Melchor, M.; Braga, A. A.; Lledos, A.; Ujaque, G.; Maseras, F. Computational  
605 perspective on Pd-catalyzed C-C cross-coupling reaction mechanisms. *Acc. Chem. Res.* **2013**, *46*,  
606 (11), 2626-2634.
- 607 (35) Li, Y.; Shi, X.; Zhang, Q.; Hu, J.; Chen, J.; Wang, W. Computational evidence for the  
608 detoxifying mechanism of epsilon class glutathione transferase toward the insecticide DDT.  
609 *Environ. Sci. Technol.* **2014**, *48*, (9), 5008-5016.
- 610 (36) Sadowsky, D.; McNeill, K.; Cramer, C. J. Dehalogenation of aromatics by nucleophilic  
611 aromatic substitution. *Environ. Sci. Technol.* **2014**, *48*, (18), 10904-10911.
- 612 (37) Pati, S. G.; Kohler, H. P.; Pabis, A.; Paneth, P.; Parales, R. E.; Hofstetter, T. B. Substrate  
613 and enzyme specificity of the kinetic isotope effects associated with the dioxygenation of  
614 nitroaromatic contaminants. *Environ. Sci. Technol.* **2016**, *50*, (13), 6708-6716.
- 615 (38) Himo, F. Recent trends in quantum chemical modeling of enzymatic reactions. *J. Am. Chem.*  
616 *Soc.* **2017**, *139*, (20), 6780-6786.
- 617 (39) Schechter, A.; Malik, N.; Haffner, D.; Smith, S.; Harris, T. R.; Paepke, O.; Birnbaum, L.  
618 Bisphenol A (BPA) in U.S. food. *Environ. Sci. Technol.* **2010**, *44*, (24), 9425-9430.
- 619 (40) Im, J.; Loffler, F. E. Fate of Bisphenol A in terrestrial and aquatic environments. *Environ.*  
620 *Sci. Technol.* **2016**, *50*, (16), 8403-8416.

- 621 (41) Ji, L.; Schuurmann, G. Computational evidence for alpha-nitrosamino radical as initial  
622 metabolite for both the P450 dealkylation and denitrosation of carcinogenic nitrosamines. *J. Phys.*  
623 *Chem. B* **2012**, *116*, (2), 903-912.
- 624 (42) Ji, L.; Schuurmann, G. Model and mechanism: N-hydroxylation of primary aromatic amines  
625 by cytochrome P450. *Angew. Chem. Int. Ed.* **2013**, *52*, (2), 744-748.
- 626 (43) Zhang, J.; Ji, L.; Liu, W. *In Silico* prediction of cytochrome P450-mediated  
627 biotransformations of xenobiotics: a case study of epoxidation. *Chem. Res. Toxicol.* **2015**, *28*, (8),  
628 1522-1531.
- 629 (44) Kepp, K. P. Heme: From quantum spin crossover to oxygen manager of life. *Coord. Chem.*  
630 *Rev.* **2017**, *344*, 363-374.
- 631 (45) Lee, C. T.; Yang, W. T.; Parr, R. G. Development of the Colle-Salvetti correlation-energy  
632 formula into a functional of the electron-density. *Physical Review B* **1988**, *37*, (2), 785-789.
- 633 (46) Becke, A. D. Density-functional thermochemistry .3. The role of exact exchange. *J. Chem.*  
634 *Phys.* **1993**, *98*, (7), 5648-5652.
- 635 (47) Hay, P. J.; Wadt, W. R. Abinitio Effective Core Potentials for Molecular Calculations -  
636 Potentials for the Transition-Metal Atoms Sc to Hg. *J. Chem. Phys.* **1985**, *82*, (1), 270-283.
- 637 (48) Kumar, D.; de Visser, S. P.; Shaik, S. How does product isotope effect prove the operation  
638 of a two-state "rebound" mechanism in C-H hydroxylation by cytochrome P450? *J. Am. Chem.*  
639 *Soc.* **2003**, *125*, (43), 13024-13025.

640 (49) Porro, C. S.; Kumar, D.; de Visser, S. P. Electronic properties of pentacoordinated heme  
641 complexes in cytochrome P450 enzymes: search for an Fe(I) oxidation state. *Phys. Chem. Chem.*  
642 *Phys.* **2009**, *11*, (43), 10219-10226.

643 (50) Strickland, N.; Harvey, J. N. Spin-forbidden ligand binding to the ferrous-heme group: Ab  
644 initio and DFT studies. *J. Phys. Chem. B* **2007**, *111*, (4), 841-852.

645 (51) Altun, A.; Breidung, J.; Neese, F.; Thiel, W. Correlated Ab Initio and Density Functional  
646 Studies on H<sub>2</sub> Activation by FeO(.). *J. Chem. Theory Comput.* **2014**, *10*, (9), 3807-3820.

647 (52) Ogliaro, F.; Harris, N.; Cohen, S.; Filatov, M.; de Visser, S. P.; Shaik, S. A model "rebound"  
648 mechanism of hydroxylation by cytochrome P450: Stepwise and effectively concerted pathways,  
649 and their reactivity patterns. *J. Am. Chem. Soc.* **2000**, *122*, (37), 8977-8989.

650 (53) Tao, J.; Perdew, J. P.; Staroverov, V. N.; Scuseria, G. E. Climbing the density functional  
651 ladder: nonempirical meta-generalized gradient approximation designed for molecules and solids.  
652 *Phys. Rev. Lett.* **2003**, *91*, (14), 146401.

653 (54) Staroverov, V. N.; Scuseria, G. E.; Tao, J. M.; Perdew, J. P. Comparative assessment of a  
654 new nonempirical density functional: Molecules and hydrogen-bonded complexes. *J. Chem. Phys.*  
655 **2003**, *119*, (23), 12129-12137.

656 (55) Perdew, J. P.; Wang, Y. Accurate and simple analytic representation of the electron-gas  
657 correlation energy. *Phys Rev B Condens Matter* **1992**, *45*, (23), 13244-13249.

658 (56) Becke, A. D. Density-functional exchange-energy approximation with correct asymptotic-  
659 behavior. *Physical Review A* **1988**, *38*, (6), 3098-3100.

660 (57) Adamo, C.; Barone, V. Exchange functionals with improved long-range behavior and  
661 adiabatic connection methods without adjustable parameters: The mPW and mPW1PW models. *J.*  
662 *Chem. Phys.* **1998**, *108*, (2), 664-675.

663 (58) Zhao, Y.; Truhlar, D. G. A new local density functional for main-group thermochemistry,  
664 transition metal bonding, thermochemical kinetics, and noncovalent interactions. *J. Chem. Phys.*  
665 **2006**, *125*, (19), 194101.

666 (59) Cao, X. Y.; Dolg, M.; Stoll, H. Valence basis sets for relativistic energy-consistent small-  
667 core actinide pseudopotentials. *J. Chem. Phys.* **2003**, *118*, (2), 487-496.

668 (60) Miertus, S.; Scrocco, E.; Tomasi, J. Electrostatic interaction of a solute with a continuum -  
669 a direct utilization of abinitio molecular potentials for the prevision of solvent effects. *Chem. Phys.*  
670 **1981**, *55*, (1), 117-129.

671 (61) Ogliaro, F.; de Visser, S. P.; Cohen, S.; Kaneti, J.; Shaik, S. The experimentally elusive  
672 oxidant of cytochrome P450: a theoretical "trapping" defining more closely the "real" species.  
673 *ChemBioChem* **2001**, *2*, (11), 848-851.

674 (62) Marenich, A. V.; Cramer, C. J.; Truhlar, D. G. Universal solvation model based on solute  
675 electron density and on a continuum model of the solvent defined by the bulk dielectric constant  
676 and atomic surface tensions. *J. Phys. Chem. B* **2009**, *113*, (18), 6378-6396.

677 (63) Grimme, S. Semiempirical GGA-type density functional constructed with a long-range  
678 dispersion correction. *J. Comput. Chem.* **2006**, *27*, (15), 1787-1799.

679 (64) Williams, P. A.; Cosme, J.; Vinkovic, D. M.; Ward, A.; Angove, H. C.; Day, P. J.; Vonnrhein,  
680 C.; Tickle, I. J.; Jhoti, H. Crystal structures of human cytochrome P450 3A4 bound to metyrapone  
681 and progesterone. *Science* **2004**, *305*, (5684), 683-686.

682 (65) Frisch, M. J., et al., Gaussian 09, revision D.01, Gaussian, Inc.: Wallingford, CT, 2013. See  
683 Supporting Information.

684 (66) Shaik, S.; Kumar, D.; de Visser, S. P. Valence bond modeling of trends in hydrogen  
685 abstraction barriers and transition states of hydroxylation reactions catalyzed by cytochrome P450  
686 enzymes. *J. Am. Chem. Soc.* **2008**, *130*, (31), 10128-10140.

687 (67) Lonsdale, R.; Harvey, J. N.; Mulholland, A. J. Inclusion of Dispersion Effects Significantly  
688 Improves Accuracy of Calculated Reaction Barriers for Cytochrome P450 Catalyzed Reactions. *J.*  
689 *Phys. Chem. Lett.* **2010**, *1*, (21), 3232-3237.

690 (68) Kolvenbach, B.; Schlaich, N.; Raoui, Z.; Prell, J.; Zuhlke, S.; Schaffer, A.; Guengerich, F.  
691 P.; Corvini, P. F. Degradation pathway of bisphenol A: does *ipso* substitution apply to phenols  
692 containing a quaternary alpha-carbon structure in the para position? *Appl. Environ. Microbiol.*  
693 **2007**, *73*, (15), 4776-4784.

694 (69) Kohler, H. P. E.; Gabriel, F. L. P.; Giger, W. *Ips*o-substitution - A novel pathway for  
695 microbial metabolism of endocrine-disrupting 4-nonylphenols, 4-alkoxyphenols, and bisphenol A.  
696 *Chimia* **2008**, *62*, (5), 358-363.

697 (70) Gabriel, F. L.; Cyris, M.; Giger, W.; Kohler, H. P. *Ips*o-substitution: a general biochemical  
698 and biodegradation mechanism to cleave alpha-quaternary alkylphenols and bisphenol A. *Chem.*  
699 *Biodivers.* **2007**, *4*, (9), 2123-2137.

700 (71) Schmidt, J.; Kotnik, P.; Trontelj, J.; Knez, Z.; Masic, L. P. Bioactivation of bisphenol A and  
701 its analogs (BPF, BPAF, BPZ and DMBPA) in human liver microsomes. *Toxicol. In Vitro* **2013**,  
702 *27*, (4), 1267-1276.

703 (72) Anslyn, E. V.; Dougherty, D. A. *Modern Physical Organic Chemistry*. University Science  
704 Books: Sausalito, CA, 2006.

705 (73) Drug Metabolism Prediction. In Kirchmair, J., Ed. John Wiley & Sons: Weinheim, **2014**.

706 (74) Kirchmair, J.; Goller, A. H.; Lang, D.; Kunze, J.; Testa, B.; Wilson, I. D.; Glen, R. C.;  
707 Schneider, G. Predicting drug metabolism: experiment and/or computation? *Nat. Rev. Drug*  
708 *Discov.* **2015**, *14*, (6), 387-404.

709 (75) Meerts, I. A.; Letcher, R. J.; Hoving, S.; Marsh, G.; Bergman, A.; Lemmen, J. G.; van der  
710 Burg, B.; Brouwer, A. In vitro estrogenicity of polybrominated diphenyl ethers, hydroxylated  
711 PDBEs, and polybrominated bisphenol A compounds. *Environ. Health Perspect.* **2001**, *109*, (4),  
712 399-407.

713 (76) Connor, K.; Ramamoorthy, K.; Moore, M.; Mustain, M.; Chen, I.; Safe, S.; Zacharewski,  
714 T.; Gillesby, B.; Joyeux, A.; Balaguer, P. Hydroxylated polychlorinated biphenyls (PCBs) as  
715 estrogens and antiestrogens: Structure-activity relationships. *Toxicol. Appl. Pharmacol.* **1997**, *145*,  
716 (1), 111-123.

717 (77) Ricken, B.; Corvini, P. F. X.; Cichocka, D.; Parisi, M.; Lenz, M.; Wyss, D.; Martinez-  
718 Lavanchy, P. M.; Mueller, J. A.; Shahgaldian, P.; Tulli, L. G.; Kohler, H.-P. E.; Kolvenbach, B.  
719 A. *ipso*-Hydroxylation and subsequent fragmentation: a novel microbial strategy to eliminate  
720 sulfonamide antibiotics. *Appl. Environ. Microbiol.* **2013**, *79*, (18), 5550-5558.

721

722

723

724 **TOC GRAPHIC**

725



726

727